IS-PORTO 2023 PROCEEDINGS

Proceedings of the 8th International Symposium on DEFORMATION CHARACTERISTICS OF GEOMATERIALS Porto, 3rd - 6th September 2023

Effect of large particle content on strength and failure mode of binary granular mixture in shear under plane strain condition

Masato Taue[1], *Yukio* Nakata[1] and Shintaro Kajiyama[2]

[1]*Yamaguchi University, Graduate school of science and technology for innovation, 2-16-1, Tokiwadai, Ube, Yamaguchi, 755-0097 Japan*
2University of Yamanashi, Graduate Faculty of Interdisciplinary Research, 4-4-37, Takeda, Kofu, Yamanashi, 400-8511 Japan
[#]*Corresponding author: mtaue2022@gmail.com*

ABSTRACT

The strength and failure modes of binary granular mixture composed of two different sized particles, such as gravel and sand, vary depending on the content of gravel (large particle content). The binary granular mixture structures are classified into small particle skeleton structure, intermediate skeleton structure, and large particle skeleton structure, depending on the large particle content. The authors propose a microscopic model to evaluate the range of large particle content in the intermediate skeleton structure, and confirm its applicability in Angle of reposed experiment. Parameters obtained from the experiment, such as " peak principal stress difference" and " principal stress difference at large axial strain" as strength, " shear band slip angle" and "shear band width " as failure mode, were discussed for large particle content. The results showed that the large-particle content of the intermediate skeleton ranged from 8.7% ~ 52.7% for the peak principal stress difference, 3.2% ~ 44.1% for the principal stress difference at large axial strain, 12.0% ~ 77.3% for the shear band slip angle, and 4.1% ~ 81.2% for the shear band width. The microscopic model calculated range for the intermediate skeleton structure was 2.3%~66.4%, which is generally wider than the experimental results under confining pressure. The microscopic model gives the range of the initial (sedimentary) state of the intermediate skeleton structure. It is inferred that the range of the intermediate skeleton structure narrows with increasing confining pressure. Therefore, the microscopic model should take into account the effect of confining pressure.

Keywords: plane strain shear test; PIV.

1. Introduction

The strength and failure modes of soils composed of two different particle sizes, such as gravel and sand, vary depending on the gravel content. A unique type of such soil is "coral gravel sand mixture," in which coral gravel is mixed into the sand as gravel. Coral gravels have a peculiar particle shape and are fragile (Watabe et al. 2015). The effect of this fragility appears in soil behavior at certain gravel content rates (Watabe et al. 2017). For this reason, understanding the relationship between gravel content and soil properties is very important. Binary granular mixtures consisting of large and small particles can clearly capture the effect of large particle content. The binary granular mixture is classified into small particle skeleton structure, intermediate skeleton structure, and large particle skeleton structure, depending on the large particle content (Ueda et al. 2011). The boundary of each is defined by the large particle content. The boundary between the small particle skeleton structure and the intermediate skeleton structure is called "Limit large particle content of small particle skeleton structure", and that between the intermediate skeleton structure and the large particle skeleton structure is called "Limit large particle content of large particle skeleton structure". The authors propose a microscopic model to evaluate the respective limit large particle content and show that the model works in Angle of reposed experiment where the confining pressure is very low (Taue et al. 2022).

In this study, plane strain compression test and image analysis (PIV) will be performed on binary granular mixtures with various large particle contents. Parameters obtained from the experiments, such as "principal stress difference" as strength, "shear band slip angle" and "shear band width" as failure mode, will be discussed for large particle content. Based on this, the range of large particle content in the intermediate skeleton structure is determined and the applicability of the microscopic model is evaluated. In this study, gravel is represented as large particles and sand as small particles for convenience.

2. Skeleton structure model and theoretical equation of microscopic model

Lade et al. (1998) proposed a skeleton structure model and a limit large particle content of large particle skeleton structure V_L^a%. In addition, Ueda et al. (2011) proposed a skeleton structure model and a limit large particle content of small particle skeleton structure V_L^b%,

for a spherical mixture of two species. The authors (Taue et al. 2022) proposed a skeleton structure model (Fig.1) and equations (1) ~ (3) that take into account the shape and anisotropy of large particles.

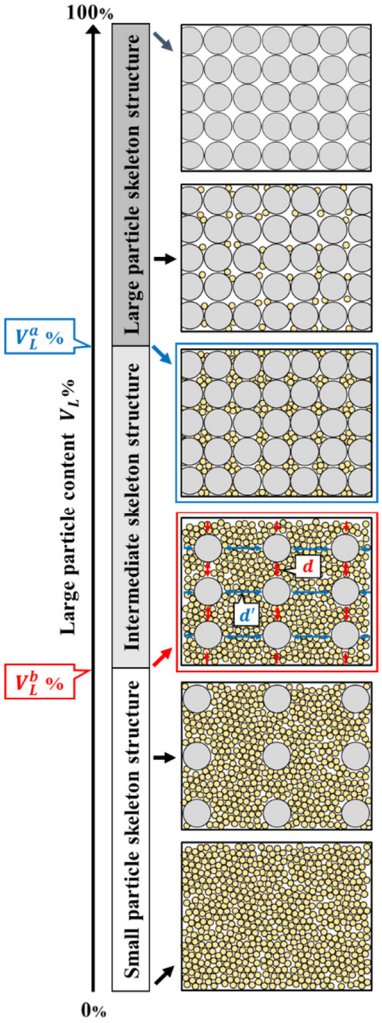

Figure 1. Skeleton structure model of microscopic model

$$V_L^b = \frac{100D_L^3(1+e_S)}{(D_L+d')(D_L+mD_S)(1+e_L)+D_L^3e_S} \quad (1)$$

$$d' = (-7.989e_S + 9.88)L \quad (2)$$

$$V_L^a = \frac{100(1+e_S)}{e_L+e_S+1} \quad (3)$$

Here, the symbols in the figure and in the equation are explained. D_L is the diameter of the large particle, D_S is the diameter of the small particle, e_L is the void ratio of the large particle sample, e_S is the void ratio of the small particle sample, $m(=2)$ is a dimensionless parameter that is the distance between large particles in the direction of maximum principal stress divided by the diameter of a small particle, $d(=mD_S)$ is the distance between large particles in the direction of maximum principal stress, d' is the distance between large particles in the direction of minimum principal stress, and L is the maximum length of large particle.

The skeleton structure model and Equations (1)~(3) have been shown to work at very low confining pressures, such as angle of repose. However, it has not been confirmed whether these work for strength and failure modes under confining pressure. In this study, the applicability of the model and equations will be clarified by plane strain compression test.

3. Plane strain compression test for binary granular mixture

3.1. Soil samples

Fig. 2 shows photographs of the large particle and small particle sample. Table 1 shows the physical properties of the large particle and small particle sample. The large particle sample is Ube silica sand and the small particle sample is Toyoura silica sand.

Figure 2. Ube silica sand (large particle) and Toyoura silica sand (small particle)

Table 1. Physical properties of samples

	Ube silica sand (Large particle)	Toyoura silica sand (Small particle)
Soil particle density	2.626 g/cm^3	2.635 g/cm^3
Average particle size	2.32 mm	0.220 mm
Particle size ratio	10.5	

3.2. Plane strain compression test

3.2.1. Test equipment and test procedure

A Plane strain testing apparatus (Fig.3, Fig.4) was used for the experiments. The size of the specimen is 80 mm long, 60 mm wide, and 160 mm high. The specimen can be observed during the test through an acrylic window. During static shear, the lower pedestal moves from side to side. The purpose is to prevent shear stress from being applied to the specimen. The test procedure is shown below.

1. The specimen was rammed with a rammer 10 times per layer. The specimen consists of 10 layers.
2. Isotropic consolidation was performed at a confining pressure of 100 kPa.
3. Static shear was applied at a confining pressure of 100 kPa and a strain rate of 0.1%/min up to 15% axial strain. An overall image of the specimen was taken every 0.1% strain.

Steps 1 through 3 were repeated with different percentages of large particles in the binary granular mixture samples. However, no experiments were conducted on samples with a large particle content of 70% or greater. This is because the small particles could

not fill the gaps formed by the large particles when the large particle content was greater than 70%, making it impossible to create a uniform binary granular mixture sample.

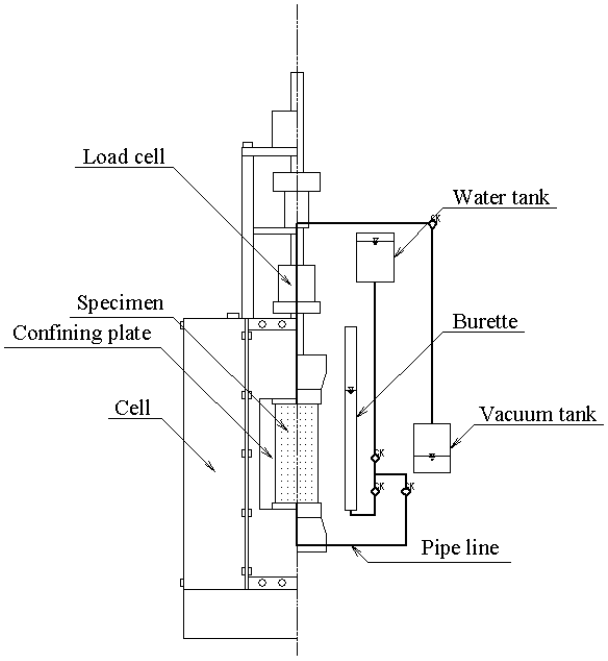

Figure 3. Plane strain testing apparatus (front view)

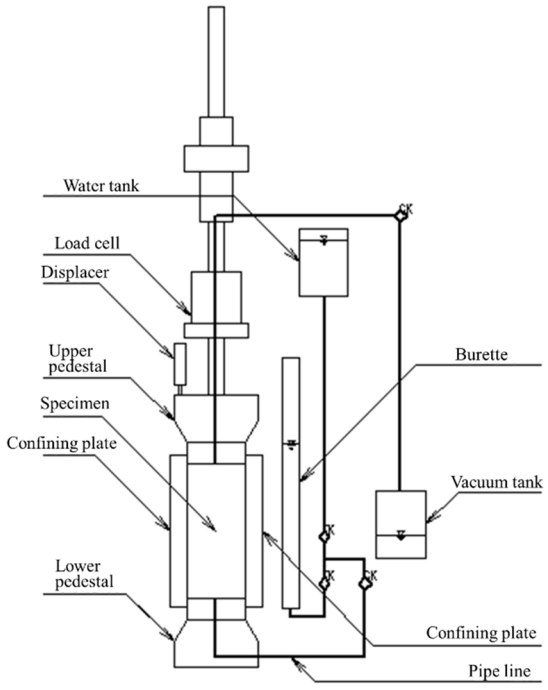

Figure 4. Plane strain testing apparatus (side view)

3.2.2. Test results

Fig.5 shows the stress-strain relationship. The low large particle content cases are in the bluish colors, while the high large particle content cases are in the reddish colors.

The stress-strain relationship for 0% large particle content (darkest coldest color) is analyzed. The principal stress difference reached its peak strength (approximately 550 kPa) at an axial strain of approximately 1.5%. Furthermore, it reaches approximately 400 kPa around 3% axial strain. The volumetric strain showed contraction at 0~1% axial strain, expansion at 1~3% axial strain, and contraction again above 3%.

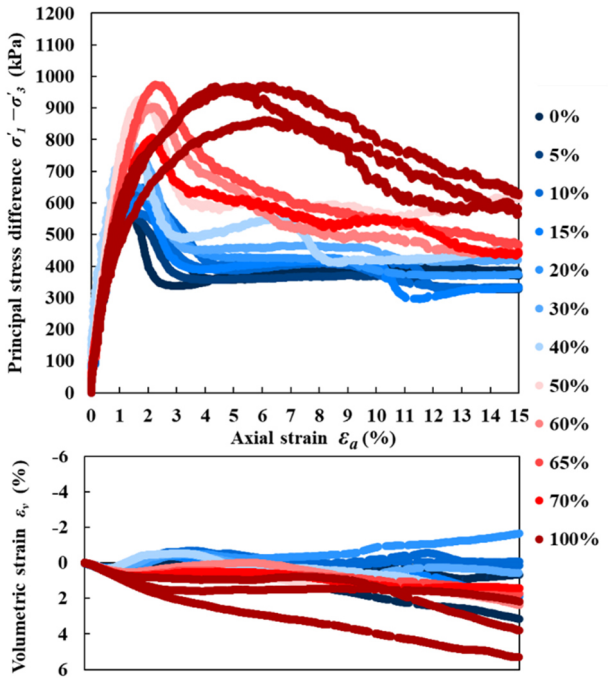

Figure 5. Stress-strain relationship

The stress-strain relationship for 100% large particle content (darkest warm color) is analyzed. The principal stress difference reached its peak strength (about 900 kPa) at an axial strain of about 5~6%. Furthermore, at 15% axial strain, the strength reached approximately 650 kPa. The volumetric strain continued to show an approximate expansion trend. The volumetric strain shows a transition from a mild expansion behavior to a contraction trend. The volumetric strain at 100% large particle content shows a larger variation than the volumetric strain at 0% large particle content.

Focus on results between 0% and 100% large particle content. As the large particle content increases, the peak strength value approaches the peak strength at 100% large particle content. This trend is the same for the axial strain at which the peak strength appears.

3.3. Shear band slip angle and shear band width based on image analysis

Fig.6 shows the definition of large axial strain, and Fig.7 shows an example of specimen images and image analysis results at large axial strain.

The large axial strain in Fig.6 is the axial strain of 2B-A%, where A% is the axial strain at the peak strength and B% is the axial strain at which the strength changes from a decreasing trend to a constant trend. However, when 2B-A% exceeded 15%, as shown in Fig.5 for 100% large particle content, the large axial strain was set to 15%. The blue points in the image analysis (PIV) results in Fig.7 are characteristic points of the specimen at 0% axial strain. The orange dots are characteristic points of the specimen at large axial strain.

The shear band is the area in the center one-third of the specimen where the orange characteristic points are displaced horizontally. The angle and width of the shear band were defined as the shear band slide angle and the shear band width.

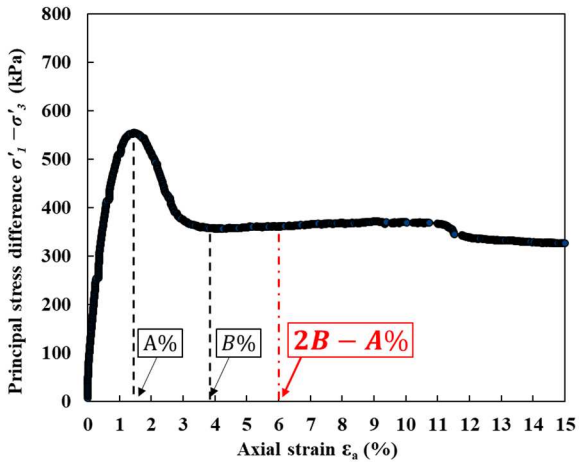

Figure 6. Definition of large axial strain

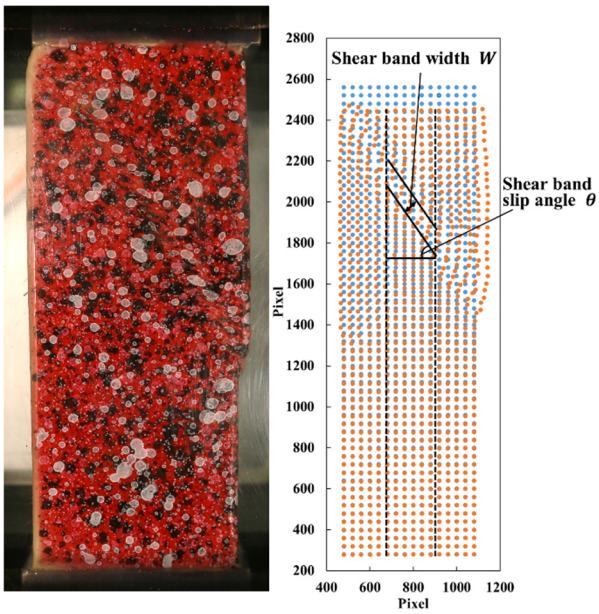

Figure 7. Specimen images and image analysis results at large axial strain

4. Limit large particle content under planar strain conditions

Fig. 8 shows the relationship between void ratio and large particle content when the specimen was created, Fig.9 shows the relationship between peak principal stress difference and large particle content, Fig.10 shows the relationship between principal stress difference and large particle content at large axial strain, Fig.11 shows the relationship between shear band slip angle and large particle content, and Figure 12 shows the relationship between shear band width and large particle content.

The meanings of the lines and colors in the figures are explained below.

The solid and dashed lines in Fig. 8 are the theoretical lines proposed in Lade's study (Lade et al. 1998); Lade's theoretical lines represent the void ratio of a binary granular mixture when the particles are ideally packed without gaps. The red and blue solid lines are the limit large particle content calculated by the microscopic model. The small particle skeleton structure is colored white, the intermediate skeleton structure is colored light gray, and the large particle skeleton structure is colored dark gray, based on the red and blue solid lines.

The dashed lines in Fig. 9 through 12 are the experimental trend lines, and the solid red and blue lines are the limit large particle content calculated by the microscopic model, as in Figure 8.

The long dashed short dashed lines are the limit large particle content determined from the experimental results. The limit large particle content of small particle skeleton structure is the large particle content when the experimental value is varied from the mean value of 0% large particle content. The limiting large particle content of large particle skeleton structure is the large particle content when the experimental value is equal to the mean value of 100% large particle content. The small particle skeleton structure is colored white, the intermediate skeleton structure is colored light gray, and the large particle skeleton structure is colored dark gray, based on the long dashed short dashed line.

4.1. Limit large particle content calculated from microscopic model

The experimental values in Fig.8 are plotted above the theoretical line as the large particle content increases. This is because the large particles are in close proximity or contact with each other, creating a gap into which the small particles cannot penetrate.

The microscopic model was calculated using Equations (1)-(3) and the following parameters for the initial state of the specimen. $e_s = 0.653$, $e_L = 0.836$, $D_L = 2.32$ mm, $D_L = 0.220$ mm, $m = 2$, and $L = 2.32$ mm.

The results showed that the Limit large particle content of small particle skeleton structure was $V_L^b = 2.3\%$ and the Limit large particle content of large particle skeleton structure was $V_L^a = 66.4\%$.

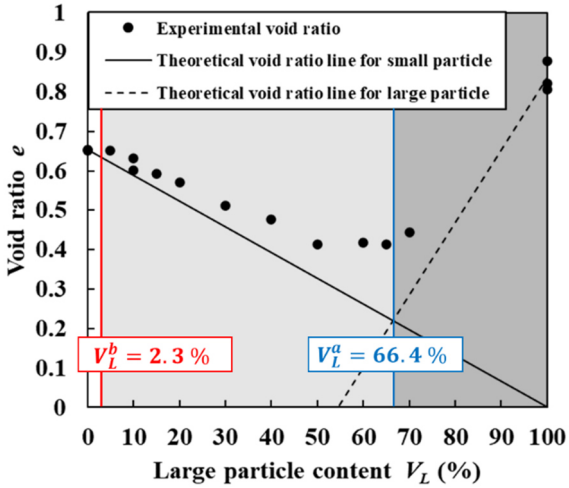

Figure 8. Relationship between void ratio and large particle content

4.2. Relationship between principal stress difference and large particle content

Fig.9 shows that the peak principal stress difference began to increase at 8.7% large particle content. At 52.7% large particle content, the peak principal stress difference equals the value at 100% large particle content. From these experimental results, the large particle content range ($V_L^b\% \sim V_L^a\%$) of the intermediate skeleton structure was determined to be 8.7%~52.7%, using the peak principal stress difference as an indicator. Compared to the limit large particle content calculated by the microscopic model, the experimental limit large particle content was 6.4% larger for $V_L^b\%$ and 13.7% smaller for $V_L^a\%$.

Fig.10 shows that the principal stress difference at large axial strain began to increase at 3.2% large particle content. At 44.1% large particle content, the principal stress difference at large axial strain equals the value at 100% large particle content. From these experimental results, the large particle content range ($V_L^b\% \sim V_L^a\%$) of the intermediate skeleton structure was determined to be 3.2%~44.1%, using the principal stress difference at large axial strain as an indicator. Compared to the limit large particle content calculated by the microscopic model, the experimental limit large particle content was 0.9% larger for $V_L^b\%$ and 22.3% smaller for $V_L^a\%$.

4.3. Relationship between shear band slip angle and large particle content

Fig.11 shows that the shear band slip angle began to decrease at 12.0% large particle content. At 77.3% large particle content, the shear band slip angle equals the value at 100% large particle content. From these experimental results, the large particle content range ($V_L^b\% \sim V_L^a\%$) of the intermediate skeleton structure was determined to be 12.0%~77.3%, using the shear band slip angle as an indicator. Compared to the limit large particle content calculated by the microscopic model, the experimental limit large particle content was 9.7% larger for $V_L^b\%$ and 10.9% larger for $V_L^a\%$. However, the sample could no longer exist as a binary granular mixture when the large particle content was over 70%. Therefore, it is possible that the experimental V_L^a was around 70% large particle content.

4.4. Relationship between shear band width and large particle content

Fig.12 shows that the shear band width began to increase at 4.1% large particle content. At 81.2% large particle content, the shear band width equals the value at 100% large particle content. From these experimental results, the large particle content range ($V_L^b\% \sim V_L^a\%$) of the intermediate skeleton structure was determined to be 4.1%~81.2%, using the shear band width as an indicator. Compared to the limit large particle content calculated by the microscopic model, the experimental limit large particle content was 1.8% larger for $V_L^b\%$ and 14.8% larger for $V_L^a\%$. However, the sample could no longer exist as a binary granular mixture when the large particle content was over 70%. Therefore, it is possible that the experimental V_L^a was around 70% large particle content.

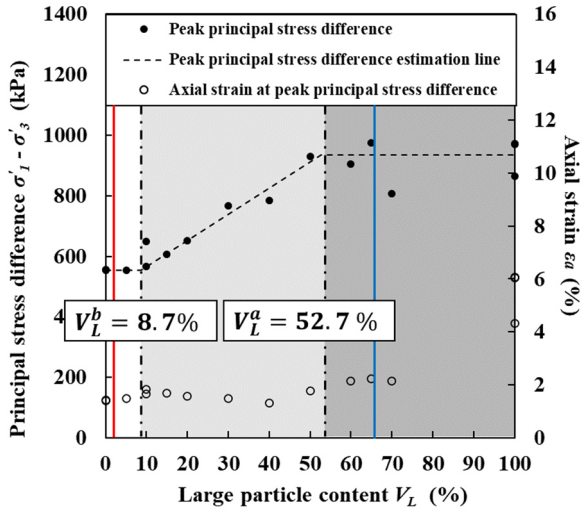

Figure 9. Relationship between peak principal stress difference and large particle content

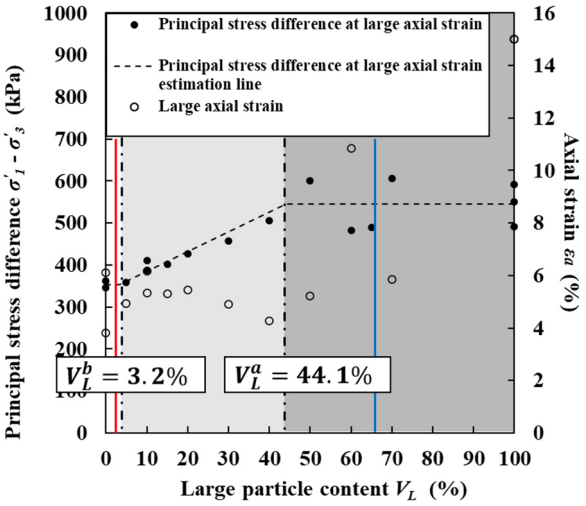

Figure 10. Relationship between principal stress difference and large particle content at large axial strain

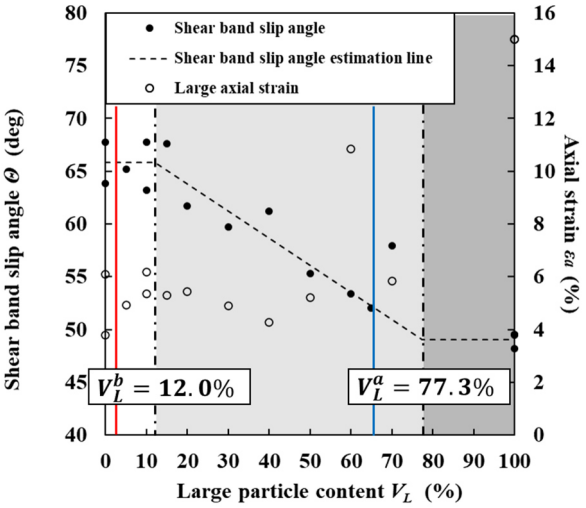

Figure 11. Relationship between shear band slip angle and large particle content

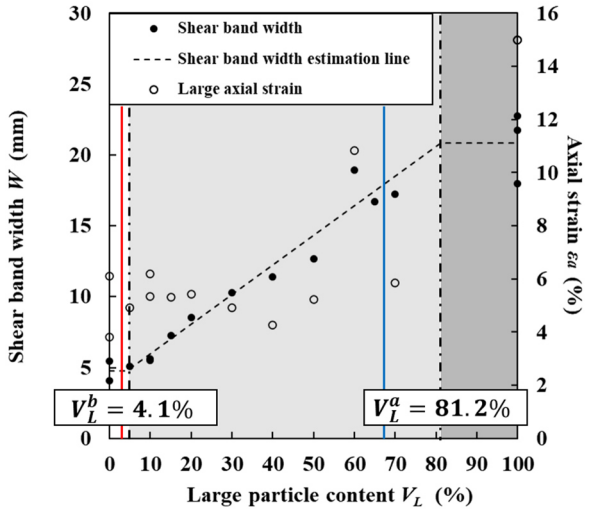

Figure 12. Relationship between shear band width and large particle content

4.5. Effect of large particle content on strength and failure mode of binary granular mixture

In 4.2 through 4.4, all of the experimental values shift from the experimental values at 0% large particle content toward the experimental values at 100% large particle content as the large particle content increases.

The trend of the experimental values, although there are errors, is divided into three parts with the limit large particle content of the microscopic model, V_L^b% and V_L^a%, as the change point. This phenomenon is caused by the proximity and contact between large particles as the large particle content increases.

In a small particle skeleton structure with a low large particle content of 0% to V_L^b%, the majority of the space is occupied by small particles. In this state, it is difficult for large particles to approach or contact each other. As a result, the small particles are the main part of the property. Therefore, the experimental values for large particle contents between 0% and V_L^b% are the same as those for large particle contents of 0%.

In the intermediate skeleton structure of V_L^b% to V_L^a%, the ratio of large particles in the space increases and the large particles come closer to each other. When large particles are close to each other, the influence of the large particles is mediated by the small particles between the large particles. This causes the influence of large particles to be felt throughout the soil. The influence of large particles becomes stronger as the large particle content increases. Therefore, the experimental values for V_L^b% to V_L^a% of large particle content approach those for 100% large particle content as the large particle content increases.

In a large particle skeleton structure with a high large particle content of V_L^a% to 100%, large particles occupy most of the space and are in complete contact with each other. As a result, the large particles are the main part of the property. Therefore, the experimental values for V_L^a% to 100% large particle content are approximately the same as those for 100% large particle content.

Finally, a microscopic model is used to evaluate the range of large particle content in the intermediate skeleton structure.

$V_L^b = 2.3\%$ and $V_L^a = 66.4\%$ calculated from the microscopic model are the range of intermediate skeleton structure for the initial sedimentary state. In 4.2 through 4.4, all V_L^b determined from experimental values under confining pressure are greater than the microscopic model's $V_L^b = 2.3\%$. The reason for this was considered to be that the influence of small particles, which occupy a majority of the space, increased as the confining pressure increased, resulting in a wider range of small particle skeleton structure.

In addition, focusing on the principal stress difference, V_L^a determined from experiment values under confining pressure are smaller than that of the microscopic model, $V_L^a = 66.4\%$. The reason for this was considered to be that the influence of large particles, which occupy a majority of the space, increased as the confining pressure increased, resulting in a wider range of large particle skeleton structure. In other words, the intermediate skeleton structure of the binary granular mixture becomes narrower as the confining pressure increases.

5. Conclusions

In this study, plane strain compression tests and image analysis (PIV) were performed on binary granular mixtures with various large particle contents. The "principal stress difference," "shear band slide angle," and "shear band width" were considered for the large particle content. Based on these, the range of large particle content in the intermediate skeleton structure was determined. The applicability of the microscopic model was also evaluated. The findings are summarized below.

- The peak principal stress difference increased from 8.7% to 52.7% for large particle content, and the principal stress difference at large axial strain increased from 3.2% to 44.1% for large particle content. From these results, the range of large particle content in the intermediate skeleton structure was determined to be 8.7% to 52.7% when the peak principal stress difference was used as an indicator, and 3.2% to 44.1% when the principal stress difference at large axial strain was used as an indicator.
- Shear band slip angle decreased with large particle content from 12.0% to 77.3%. Shear band width increased with large particle content from 4.1% to 81.2%. From these results, the large particle content range of the intermediate skeleton structure was determined to be 12.0% to 77.3% when the shear band slip angle was used as an indicator, and 4.1% to 81.2% when the shear band width was used as an indicator. However, the sample could no longer exist as a binary granular mixture when the large particle content was over 70%. Therefore, it is possible that the experimental V_L^a was around 70% large particle content.
- The range of intermediate skeleton structure calculated from the microscopic model ranged from 2.3% to 66.4%. The limit large particle content of small particle skeleton structure, V_L^b%, obtained in the experiments under confining pressure was larger than the microscopic model, V_L^b%. On the

other hand, the limit large particle content of large particle skeleton structure, V_L^a%, was smaller than that of the microscopic model, V_L^a%, in the case where the principal stress difference was used as an indicator. The microscopic model gives the intermediate skeleton structure in the initial (sedimentary) state. It was inferred that the range of large particle content in the intermediate skeleton structure is narrowed with increasing confining pressure. Therefore, in order to accurately evaluate the range of the intermediate skeleton structure, it is necessary to take into account the effect of the confining pressure in the microscopic model.

Acknowledgements

This research was supported by Grant-in-Aid for JSPS Fellows (22J15374, Masato Taue). The authors would like to express their deepest gratitude to all those involved.

References

Watabe, Y., Sassa S., Kaneko, T. and Nakata Y. "Mechanical characteristics of reconstituted coral gravel soils with different fractions of finger-coral fragments and silt matrix", Soils and Foundations, 55, 5, 1233–1242, 2015. https://doi.org/10.1016/j.sandf.2015.09.022

Watabe, Y., Sassa S., Kaneko, T. and Nakata Y. Mechanical characteristics of undisturbed coral gravel soils: The intergranular void ratio as a common governing parameter", Soils and Foundations, 57, 5, 760-775, 2017. https://doi.org/10.1016/j.sandf.2017.08.007

Ueda, T., Matsushima, T. And Yamada Y. "Effect of particle size ratio and volume fraction on shear strength of binary granular mixture", Granular Matter, 13, 731-742, 2011. (in Japanese)
https://doi.org/10.1007/s10035-011-0292-1

Taue, T., Nakata, Y. and Kajiyama, S. "Evaluation of limit large particle content of small particle skeleton structure for binary granular mixture based on microscopic model", Doboku Gakkai Ronbunshu, 78, 1, 32-44, 2022. https://doi.org/10.2208/jscejge.78.1_32

Lade, P.V., Liggio, C.D. and Yamamuro, J.A.,"Effects of nonplastic fines on minimum and maximum void ratios of sand", Geotech Test J , 21, 4, 336-347, 1998. https://doi.org/10.1520/GTJ11373J